



# HHS Public Access

Author manuscript

*Nat Photonics*. Author manuscript; available in PMC 2014 October 23.

Published in final edited form as:

*Nat Photonics*. 2013 ; 7: 987–994. doi:10.1038/nphoton.2013.278.

## Light-guiding hydrogels for cell-based sensing and optogenetic synthesis *in vivo*

Myunghwan Choi<sup>1,2</sup>, Jin Woo Choi<sup>1,3</sup>, Seonghoon Kim<sup>2</sup>, Sedat Nizamoglu<sup>1</sup>, Sei Kwang Hahn<sup>1,4</sup>, and Seok Hyun Yun<sup>1,2,\*</sup>

<sup>1</sup>Harvard Medical School and Wellman Center for Photomedicine, Massachusetts General Hospital, Boston, Massachusetts, USA.

<sup>2</sup>WCU Graduate School of Nanoscience and Technology, Korea Advanced Institute of Science and Technology, Daejeon, Korea.

<sup>3</sup>Wonkwang Institute of Interfused Biomedical Science, Department of Pharmacology, School of Dentistry, Wonkwang University, Seoul, Korea.

<sup>4</sup>Department of Materials Science and Engineering, Pohang University of Science and Technology, Pohang, Korea.

### Abstract

Polymer hydrogels are widely used as cell scaffolds for biomedical applications. While the biochemical and biophysical properties of hydrogels have been extensively investigated, little attention has been paid to their potential photonic functionalities. Here, we report cell-integrated polyethylene glycol-based hydrogels for *in-vivo* optical sensing and therapy applications. Hydrogel patches containing cells were implanted in awake, freely moving mice for several days and shown to offer long-term transparency, biocompatibility, cell-viability, and light-guiding properties (loss: <1 dB/cm). Using optogenetic, glucagon-like peptide-1 (GLP-1) secreting cells, we conducted light-controlled therapy using the hydrogel in a mouse model with type-2 diabetes and attained improved glucose homeostasis. Furthermore, real-time optical readout of encapsulated heat-shock-protein-coupled fluorescent reporter cells made it possible to measure the nanotoxicity of cadmium-based bare and shelled quantum dots (CdTe; CdSe/ZnS) *in vivo*.

---

Users may view, print, copy, download and text and data- mine the content in such documents, for the purposes of academic research, subject always to the full Conditions of use: [http://www.nature.com/authors/editorial\\_policies/license.html#terms](http://www.nature.com/authors/editorial_policies/license.html#terms)

\*Corresponding Author: S. H. Andy Yun, Ph.D., Associate Professor, Harvard University, 65 Landsdowne St. UP-525, Cambridge, MA 02139, USA, Tel: 1-617-768-8704, [syun@hms.harvard.edu](mailto:syun@hms.harvard.edu).

#### Author contributions

M.C. and S.H.Y. designed experiments. M.C. performed experiments. J.W.C., S.K., and S.N. provided materials. M.C., S.K., S.K.H., and S.H.Y. analyzed data. M.C. and S.H.Y. wrote the manuscript with inputs from authors.

#### Additional information

Supplementary information is available in the online version of the paper. Correspondence and requests for materials should be addressed to [syun@hms.harvard.edu](mailto:syun@hms.harvard.edu) (S.H.Y.).

#### Competing financial interests

The authors declare no competing financial interests.

## Keywords

Optical waveguide; Hydrogel; Biosensor; Optogenetics; Synthetic biology; Photomedicine

As the autonomous building block of the body, cells have amazing abilities to sense their local environment and respond to external chemical and physical cues<sup>1</sup>. In addition, cells secrete cytokines and hormones that are critical for homeostasis and also useful for therapeutic purposes<sup>2</sup>. There have been considerable efforts to employ these cellular functions in medicine for diagnosis and treatment, for example, by injecting specialized cells or implanting bioengineered cells in patients<sup>3,4</sup>. In this cell-based approach, it is desired and often necessary to communicate with these cells for receiving sensor signals from the cells or sending regulatory control signals to the cells. For this purpose, light offers an attractive means of communication in the biological system. Various light-sensitive molecules and genetic engineering tools are available to build optical interfaces into cells<sup>5,6</sup>. Fluorescent or bioluminescent proteins can be integrated into a specific pathway of endogenous sensing machinery for highly selective sensing<sup>7</sup>. Photoactive proteins, such as channel rhodopsin and melanopsin, can be coupled with the pathway leading to light-driven production of therapeutic substances with its timing and dose control by light<sup>8-11</sup>.

Despite the great promise of light-mediated, cell-based sensing and therapy, one of the fundamental challenges in this field is the high optical loss in biological tissue due to scattering and absorption<sup>12</sup>. The  $1/e$  optical penetration depth,  $L_e$ , at which the light intensity drops to  $1/e$  level (37%), in soft tissue is less than 1 mm for the visible and near infrared range<sup>13</sup>. Transdermal light delivery by external illumination has shown to be viable for an optogenetic release of a therapeutic protein from the cells implanted subcutaneously in mice<sup>9</sup>. While this approach is feasible in small experimental animals through their thin skin, its application to humans is unlikely because it would require too high optical energy beyond the safety threshold ( $4 \text{ W/cm}^2$ ) of the tissue. Endoscopes can provide minimally invasive access into the body. But this approach limits the location of cells to near the surfaces of internal organs, such as the mucosal layer of the gastrointestinal tracts, and is not suitable for continuous operation over an extended period of time (e.g. several days). Another challenge in this endeavor is the need to illuminate the implanted cells and collect light from them when the cells are dispersed widely in space. While a point illumination by an optical fiber is adequate for certain scenarios, such as focal optogenetic control in the brain<sup>14</sup>, most applications demand a sufficient number of cells distributed over dimensions much larger than the typical  $1/e$  optical attenuation distance in order of 1 mm, for which point illumination by conventional optical fibers is not suited<sup>15</sup>.

Here, we demonstrate that hydrogels, which are commonly used as scaffolds for cell culture *in vitro* and implantation *in vivo*<sup>16</sup>, can be designed, fabricated, and used for efficient light delivery and collection, as well as cell encapsulation<sup>17,18</sup>. We show that cell-containing optical hydrogels can be implanted *in vivo* for an extended period and serve as an optical communication channel between encapsulated cells and an external light source and detector via a strand of thin flexible optical fiber (Fig. 1). We apply this novel approach to real-time

cell-based toxicity sensing and light-controlled optogenetic production of an anti-diabetic glucagon-like peptide-1 (GLP-1) in live mice.

## Results

Polymer hydrogels has been extensively studied as cellular scaffolds. The porous aqueous polymeric network of hydrogels allows small molecules, such as glucose, oxygen, and secretory proteins, to be efficiently exchanged with surrounding host tissues by diffusion for the long-term survival of encapsulated cells. The cellular adhesiveness and biodegradability of hydrogels can be readily modified with the chemical compositions and fabrication parameters. The physicochemical, biomechanical, and biological properties of the hydrogels based on various synthetic or natural polymers have been characterized, and numerous recipes to optimize these properties have been established<sup>19,20</sup>. However, relatively little has been studied about the optimization of their optical properties. In the present study, we chose polyethylene glycol (PEG)-based hydrogels, widely used for various biomedical applications<sup>21</sup>. We began our study by finding optimal design parameters, such as molecular weights, water contents, and the shape of hydrogels, for desired functional properties. PEG-based hydrogels were formed by UVinduced polymerization and crosslinking of PEG diacrylate (PEGDA) precursor solutions mixed with photoinitiators (Irgacure, 0.05% w/v).

### Optical transparency of PEG hydrogels

The ability to control the transparency of hydrogels is required for their photonic applications. To determine optimal compositions, we measured the optical loss spectra of hydrogels prepared by using PEGDA with various molecular weights (MW) of 0.5, 2, 5, and 10 kDa, respectively, at the same concentration of 10% weight/volume (w/v) (Fig. 2a). PEG hydrogels with a MW of 0.5 kDa in standard 1-cm cuvettes were white opaque indicating strong uniform scattering across the visible spectrum. With increasing MW, PEG hydrogels became transparent. Attenuation spectroscopy confirmed the strong dependency on the MW of the precursor polymer. PEG hydrogels of 0.5 kDa had an optical loss of about 25 dB/cm (i.e.  $L_e=1.8$  mm) in the visible range (400–700 nm) (Fig. 2b). When the PEGDA concentration increased to 60% w/v or higher, hydrogels became noticeably more transparent (Supplementary Fig. S1). However, these concentrations were not adequate for cell encapsulation because of the low water contents (<90%). Furthermore, the hydrogels became increasingly stiffer with concentration, which can reduce cell viability and cause undesirable tissue damage when implanted *in vivo*. Hydrogels prepared with 2, 5, and 10 kDa PEGDA exhibited much lower optical loss. In the blue to green range of 450–550 nm, the average loss was measured to be 0.68 dB/cm ( $L_e=6.4$  cm) for 2 kDa, 0.23 dB/cm ( $L_e=19$  cm) for 5 kDa, and 0.17 dB/cm ( $L_e=26$  cm) for 10 kDa PEGDA. Hydrogels were fabricated in rectangular custom-made glass molds by *in situ* photo-induced crosslinking (Supplementary Fig. S2). The typical dimension of the PEG hydrogels was 4 mm in width, 1 mm in height, and 10–40 mm in length. The fabricated 0.5-kDa hydrogels (10% w/v) were semi-opaque as seen through the 1-mm thickness, whereas the 5-kDa hydrogels were markedly more transparent (Fig. 2c).

## Effects of swelling on physical properties

To investigate the stability of the optical properties of hydrogels in aqueous environment, we performed a swelling test. The hydrogels were immersed in phosphate buffered saline (PBS) for 12 h, and the fractional weight increase due to water absorption was measured<sup>22</sup>. The swelling ratio increased with the MW of PEGDA from 0.5 to 10 kDa (Fig. 2c). The rectangular shape of the 10-kDa hydrogels were found to be severely deformed due to swelling, whereas 0.5–5 kDa hydrogels maintained their rectangular shapes with minimal distortion. Interestingly, despite the swelling all hydrogels (0.5–10 kDa) did not show any apparent changes in transparency. We also found that hydrogels became more flexible with increasing MW. While 0.5 kDa hydrogels were quite brittle, 5 kDa hydrogels were highly elastic such that they could be easily bent and twisted (Fig. 2e). Considering the excellent transparency, structural stability, and mechanical flexibility, we chose to use PEG hydrogels with 5 kDa MW and 10% w/v concentration throughout the studies described below.

## Light guiding in slab hydrogels

We investigated the optical guiding properties of slab hydrogels with a rectangular shape of 4 mm (w) × 1 mm (h) × 40 mm (l). The refractive index of 10% w/v hydrogels was estimated to be about 1.35 (the index of 100% PEG is 1.465). When a laser beam (491 nm) was launched into the hydrogel at an angle, it propagated in a zigzag path (Fig. 2f) due to total internal reflection at the hydrogel-air interfaces. For fiber-optic connection, a multimode fiber (core diameter, 100 μm; numerical aperture, 0.37) was integrated during the fabrication of hydrogels (Supplementary Fig. S2). Light from an external light source was coupled into a hydrogel via the optical fiber pigtail (Fig. 3a). The light from the optical fiber was dispersed in the cross-section of the hydrogel nearly uniformly after a several-mm-long diffraction region (Fig. 3b). The light propagated all the way to the distal end of the 4 cm-long hydrogel waveguide and exited through the end surface (Fig. 3b).

## Light collection by hydrogels

We also tested the property of hydrogel waveguide for collecting the light that could be generated from a hydrogel or from the surrounding tissue and delivering it to a photodetector. We measured the amount of fluorescence light collected from a green-fluorescent plate or dye solution (FITC; 5% w/v) at a varying distance, with and without a hydrogel in between (Fig. 3c). The excitation light (455 nm) was delivered from a laser through the pigtail fibers. The length of hydrogel was varied by cutting it from 40 mm to 30, 20, 10 and 5 mm, respectively, in length ( $L$ ). The collection efficiency of the optical fiber alone decreased with  $1/L^2$ , as expected from the geometry. On the other hand, with hydrogels the collection efficiency followed a linear decay function with  $1/L$  (Fig. 3d). The difference in ratio, or the enhancement factor, increased linearly with the length of the hydrogel, which was about 80-fold (19 dB) for 4-cm-long hydrogels (Fig. 3e). Taken together, our results demonstrate the desired optical functions of the hydrogel both for transmitting light from an external source to the inside of the hydrogel and for delivering light from the hydrogel to an external detector.

### Cell-encapsulated hydrogels

For cell encapsulation, HeLa cells were mixed into the precursor PEGDA solution, with Arg-Gly-Asp (RGD) peptides (1 mM), prior to crosslinking. Due to their refractive index profile (1.35–1.36 in the nucleus and 1.36–1.39 in cytoplasm<sup>23</sup>), the cells in the hydrogel refract and scatter light. Absorption spectroscopy showed the scattering-induced loss of cell-encapsulated hydrogels (Fig. 3f). For a given cell density, the attenuation was relatively uniform over the visible to near infrared range (400–900 nm) with slight decreases with the wavelength. The attenuation coefficients were found to increase nonlinearly with the cell density (Fig. 3g), which reached as high as 2.4 dB/cm ( $L_e=1.8$  cm) with  $5 \times 10^6$  cells/ml in the wavelength range of 450–500 nm. The cell density of about  $10^6$  cells/ml was determined to be optimal for 4-cm-long hydrogels, at which the loss is less than 1 dB/cm and the 1/e attenuation length ( $L_e=5.6$  cm) is comparable to the length of the hydrogel. At this cell density, a hydrogel with  $1 \times 4 \times 40$  mm<sup>3</sup> (0.16 cm<sup>3</sup>) could contain up to 160,000 cells and, without molecular absorption, carry 70% light to its distal end.

### Implantation of cell-containing hydrogel *in vivo*

Cell-containing hydrogels were implanted into the subcutaneous pocket of mice through a 1-cm long skin incision on the back (Fig. 4a). The pigtail fiber was securely cemented onto the skull to establish stable light coupling to the hydrogel while the animal is awake and moving freely (Fig. 4b; Supplementary Video S1). Light leaked out of the hydrogel to the surrounding tissue could be readily monitored through the thin skin layer (Fig. 4c). The optical intensity throughout the entire implant varied no more than 6 dB, which is slightly higher than 1 dB/cm measured in the air and is due to the contact with the tissue (index, 1.34–1.41) (Fig. 4d). By comparison, when only a multimode fiber was implanted without hydrogel, the 1/e light intensity was constrained to a small region with a diameter of 2–3 mm as seen through the skin (Figs. 4c, d). This result represents a 40-fold increase of the illumination area by the light-guiding scaffold.

The hydrogels and surrounding tissues were harvested at day 3 and day 8 after implantation (n=3). Fluorescence microscopy with cell viability probes showed that about 80% of the embedded cells were found live in the hydrogels *in vitro* after photo-crosslinking, and more than 70% and 65% of the embedded cells in the implanted hydrogels remained viable for 3 and 8 days, respectively (Fig. 4e), which was consistent with the measurement with hydrogels in a culture dish *in vitro* (Fig. 4f and Supplementary Fig. S3). The decreases of optical transmittance for 3 and 8 days *in vitro* and *in vivo* were less than 1 dB/cm (Fig. 4g). Histology suggested there were no major immune-cell infiltrations but the formation of connective tissues around the implants, which is a typical mild foreign body reaction, were observed in all, but not in sham surgery, animals (Fig. 4i). The newly formed tissues were moderately vascularized. The hydrogel implants as a whole came off from the surrounding tissues so easily during tissue harvesting, indicating lack of adhesion between the tissues and hydrogels.

### *In vivo* sensing of nanotoxicity

We applied fiber-optic cell-containing hydrogel implants for measurement of the toxicity of quantum-dot (Q-dot) *in vivo*. For sensing cellular toxicity, we employed an intrinsic cellular

cytotoxicity sensor, heat-shock-protein 70 (hsp70)<sup>24</sup>, which is activated when cells are under cytotoxic stresses, such as heavy metal ions and reactive oxygen species, and green fluorescent protein (GFP) under the hsp77 promoter. Cadmium (Cd) is a widely used heavy metal in Q-dots but can cause cytotoxic effects when released by degradation of Q-dots. The magnitude of green fluorescence from these sensor cells *in vitro* increased with the sub-lethal dose of CdCl<sub>2</sub> up to 1 μM but saturated at higher concentrations of 1–5 μM (Supplementary Fig. S4). Two types of Cd-containing Q-dots were tested: core-only CdTe and core/shell CdSe/ZnS nanoparticles. The sizes of the bare and shelled Q-dots were about 3.2 and 5.2 nm, respectively, such that they emit red fluorescence (605 nm) readily distinguishable from the green-fluorescence signal. When the cells were encapsulated in a hydrogel *in vitro*, the sensor signal increased with the concentration of CdTe Q-dots in the medium, but no noticeable change of green fluorescence was observed when CdSe/ZnS Q-dots was applied (Fig. 5a, b). This result confirmed the dramatic role of the ZnS shell in reducing cellular toxicity.

Next, we implanted cell-encapsulating hydrogels into three groups of mice, which were treated by a systemic injection of CdTe Q-dots (100 pM), CdSe/ZnS Q-dots (100 pM), and PBS only, respectively. Time-lapse fiber-optic fluorescence measurement (Supplementary Fig. S5) showed significant increase in green fluorescence in the CdTe-treated group, but not in the CdSe/ZnS-treated and control groups, at day 1 and day 2 after the treatments (Fig. 5c). To validate this measurement, we extracted the hydrogel implants at day 2 from the mice and examined with fluorescence microscopy (Fig. 5d). The total magnitude of GFP fluorescence from the cells was qualitatively consistent with the values measured *in situ* in live mice (Fig. 5e). These results represent the first real-time measurement of systemic cellular toxicity by Cd-based Q-dots and the effect of surface capping by biocompatible shells.

### Optogenetic therapy of diabetic mice

To demonstrate cell-based therapy, we used a vector construct previously developed for optogenetic synthesis of GLP-1<sup>9</sup> and generated a stably transfected cell line (Supplementary Fig. S6). Upon absorption of blue light, the light-responsive protein, melanopsin, in the plasma membrane is activated, which increases intracellular calcium and consequently activates a transcription factor, nuclear factor of activated T cell (NFAT), which drives the production of GLP-1. GLP-1 is an anti-diabetic secretory protein that promotes glucose homeostasis by stimulating glucose-dependent insulin secretion<sup>25</sup>. We first confirmed the intended function of these optogenetic cells when encapsulated in a hydrogel *in vitro*. To monitor the change in the intracellular calcium level, the optogenetic cells were loaded with a fluorescence-based calcium indicator (OGB1-AM). More than 80% of the cells illuminated by blue light showed increase of intracellular calcium within several seconds (Fig. 6a, b). The temporal kinetics of calcium signals was consistent with cells in light-exposed (ON) samples compared to non-illuminated (OFF) controls (Fig. 6c). This result confirmed the optogenetic synthesis of GLP-1 and permeability of secreted GLP-1 molecules through the crosslinked hydrogel.



To investigate the therapeutic potential of the optogenetic system, we implanted cell-containing hydrogel into chemically induced type-2 diabetic mice<sup>26</sup>. Blue light (455 nm, 1 mW) was fiber-optically delivered for 12 h after the implantation. At 48 h after the implantation, light-exposed animals (n=4) showed approximately two-fold increase in the blood GLP-1 level compared to the non-illuminated control group (Fig. 6d). To validate physiological efficacy, we performed glucose tolerance test. Following an intraperitoneal injection of glucose (1.5 g/kg), the light-treated group achieved significantly improved glucose homeostasis where the blood glucose level returned to the initial level of 14 mM in 90 min (Fig. 6e). In contrast, the blood glucose level of the non-treated group remained higher than 28 mM even after 120 min (Fig. 6e). This result demonstrates the therapeutic potential of the cell-hydrogel implant for optically controlled optogenetic synthesis in the body.

## Discussion

Recently, there has been a growing interest to develop photonics devices based on biomaterials, such as silk fibroin<sup>27</sup>, agar<sup>17</sup>, and synthetic polymers<sup>28</sup>. Various biocompatible photonic components, such as optical fibers and gratings, have been demonstrated and their optical functions were tested under *in vitro* and, to some extent, *in vivo* settings. In this study, we have used PEG-based hydrogels to demonstrate, for the first time, *in vivo* biomedical applications of cell-containing optical waveguides. We have shown that hydrogels can serve not only as a cellular scaffold but also as a bidirectional optical communication channel for encapsulated cells. Optical hydrogel implants encapsulating cells with luminescent reporters and optogenetic gene-expression machinery allowed us to perform the first real-time sensing of nanotoxicity in animals and optogenetic diabetic therapy with an optical power of only 1 mW, much more efficient than conventional transdermal delivery<sup>9</sup>.

Optical transparency is essential for most photonic applications of hydrogels. We found that the longer PEGDA polymers yielded the higher transparency after crosslinking. This general tendency may be explained by the formation of pores in crosslinked hydrogels. In solutions prior to crosslinking, the precursor PEG chains are homogeneously dispersed in water and, therefore, transparent. UV-induced polymerization reorganizes the monomer distribution following energy minimization. This can introduce spatial inhomogeneity depending on the molecular compositions and crosslinking parameters. As a distinct phenomenon, phase separation between the polymer-rich phase and the water-rich phase<sup>29</sup> can occur when the water content exceeds the maximum equilibrium level the crosslinked polymer can uptake during polymerization. The resulting pores, with sizes ranging from nano to micrometers, cause light scattering due to the refractive index contrast and reduces transparency. This mechanism explains the opaqueness of 0.5-kDa PEG hydrogels made at 10% w/v and the improved transparency at lower water contents (higher concentrations >15% w/v) (Supplementary Fig. S2).

The light guiding properties of hydrogels can be tailored for specific requirements by controlling the shape and structure of the hydrogels. For example, cell-based therapy in patients should require a sizable hydrogel to contain large number of cells to produce

physiologically relevant dose. In this case, an additional cladding layer with lower refractive index may be employed to enhance guiding. The width of the hydrogel may be tapered to compensate for cell-induced optical loss and, thereby, obtain more uniform optical intensity throughout the entire volume. Besides PEG, other polymers widely used in cell culture and tissue engineering, such as hyaluronic acid, alginate and collagen, are good candidates for optical hydrogels. Hydrogels based on these polymers have shown excellent properties for cell encapsulation. Compositional screening and optimization for optical characteristics could result in a range of material options for light-guiding hydrogels with different refractive indices. Other than a preformed hydrogel, injectable hydrogels such as thermo-responsive gels may be used to facilitate minimally invasive implantation through *in situ* gelation<sup>30</sup>. Further optimization of mechanical stability, flexibility, or biodegradation is also achievable by modifying chemical compositions or fabrication protocol<sup>31</sup>. Additionally, photodegradable group may be introduced to control biodegradation kinetics.

There remain challenges for the clinical applications of hydrogels<sup>32</sup>. First, as the amount of therapeutic substances required for systemic diseases is proportional to the body weight, larger hydrogels are required. Our data indicate that it is plausible to increase the cell density by 5-fold ( $5 \times 10^6$  cells/cm<sup>3</sup>) without lowering the optical transmission substantially, and even higher concentrations may be possible with optimized hydrogel designs. Furthermore, different host cells with enhanced transfection efficiency may be used. For example, HEK293 cells have an order-of-magnitude higher protein production rate than the HeLa cells used in our work<sup>9</sup>. Additionally, genetic and protein engineering to increase the production rate and stability of therapeutic protein will lead to a further reduced implant size<sup>33</sup>. Second, the cell-hydrogel implant should be functionally stable *in vivo* for several weeks and months depending on applications, for example, for chronic problems. Such long lifetime is currently challenging although not unattainable<sup>34</sup>. Lastly, more careful investigation of the long-term host response against implanted hydrogels is required<sup>35</sup>. All of the above issues have long been major research topics in the field of regenerative medicine and tissue engineering. Continuing progress in this field will increase the clinical potential of the hydrogel-based technique<sup>21</sup>.

The light-guiding hydrogel system can also employ non-cell-based chemical sensors and photoactive therapeutic molecules<sup>36</sup>. Although this approach does not benefit from the unique features, such as self-sustainability, of cells, it provides simplicity and allows existing molecular probes and drugs to be used in conjunction with light-guiding hydrogels.

In conclusion, we have demonstrated a new optical hydrogel waveguide, which offers excellent low-loss light-guiding properties and simultaneously meets all the requirements including long-term cell encapsulation, mechanical flexibility, and long-term transparency *in vivo*. By coupling the numerous cellular sensing and secretory protein-production pathways with optical readout and optogenetic signaling, the optical hydrogel system has a potential to be a platform technology with a broad range of applications in diagnosis and therapy.



## Methods

### Hydrogel fabrication

PEGDA (Laysan Bio) solution in PBS at concentrations between 10 and 60% (w/v) was mixed with 0.05% (w/v) photoinitiator Irgacure 2959 (Ciba)<sup>22</sup>. The solution was transferred to a custom-made glass mold and exposed to a UV lamp (365 nm, 5 mW/cm<sup>2</sup>; Spectroline) for 15 min. For fiber coupling, a multimode optical fiber (100  $\mu$ m-core, 0.37 NA; Doric Lenses) was embedded in the polymer solution at its tip (a few mm's) and aligned to the long axis of the hydrogel prior to photo-crosslinking. Epoxy was applied to reinforce the fiber-hydrogel joint. For cell encapsulation, cells in culture dish were treated with trypsin, quantified and mixed into the PEGDA solution at concentration of  $5 \times 10^5$  to  $10^6$  cells/ml prior to photo-crosslinking. The high cell-viability of this protocol was confirmed with multiple cell lines including Hela (human cervical cancer cell), HEK293T (human kidney cell), and EL4 (mouse T cell) (Supplementary Fig. S3). The crosslinked hydrogel was placed in culture medium and incubated for more than one day prior to implantation into a mouse. The cell medium was replaced at 1 h, 3 h, and every 24 h.

### Preparation of cells

Hela cell (ATCC, Manassas, VA, USA) was maintained in Dulbecco's modified Eagle's medium (DMEM) supplemented with 10% fetal bovine serum, and 1% antibiotics at 37 °C in 5% CO<sub>2</sub>. For cytotoxicity reporter cells, Hela cells were transiently transfected with an HSP70-GFP vector using Lipofectamine 2000 (Life Technologies) according to the manufacturer's protocol. After incubation overnight, the cells were trypsinized and encapsulated in a hydrogel for the sensing experiments. Optogenetic cell line was generated by stable transfection of two vectors, namely pHY42 (human melanopsin; neomycin resistant) and pHY57 (NFAT-shGLP1, NFAT driven short variant human GLP1; hygromycin resistant). Hygromycin (150 mg/ml) and G418 (800  $\mu$ g/ml) were added every other day from 48 h after introduction of the vectors for 2 weeks. Selected colonies were transferred into a 24 well plate and incubated. After being confluent, the cells dissolved in RIPA buffer containing 1% Triton- X100 and 0.1% SDS. The lysates were separated by a 10% SDS-PAGE gel and transferred to a PVDF membrane. To check the expression level of melanopsin, the membrane was tested by western blot using polyclonal antibody against human melanopsin (ab65641, Abcam). Expression of shGLP-1 was confirmed by a GLP-1 ELISA kit (Millipore). The cell lines that highly express both melanopsin and shGLP-1 were used for optogenetic experiments.

### Characterization of hydrogels

PEG hydrogels were prepared in standard 1-cm-wide poly(methyl methacrylate) (PMMA) disposable cuvettes and optical attenuation was measured using a scanning spectrophotometer (Thermo Scientific). The optical transmittance of slab hydrogels was measured through their 1-mm thickness axes by using the collimated beam from a blue continuous-wave laser (20 mW,  $\lambda = 491$  nm; Cobolt Calypso, Cobolt) and an optical power meter (1918-R, Newport). Swelling ratios, defined as the weight of dried hydrogel divided by the weight of hydrogel, were measured after placing hydrogels in PBS for 12 hours<sup>22</sup>. For cell viability test, a hydrogel was washed in serum-free medium and incubated in serum-

free medium containing calcein AM (1  $\mu\text{l/ml}$ ; Life Technologies) and ethidium bromide (2  $\mu\text{l/ml}$ ; Life Technologies) for 30 min. The hydrogel is then incubated in serum-free medium for 15 min, washed with PBS, and imaged with a fluorescence microscope (Olympus).

### Implantation

After anesthetizing a mouse by intraperitoneal injection of ketamine (100 mg/kg) and xylazine (10 mg/kg), the dorsal skin was incised over about 1 cm horizontally, and a round spatula was inserted to form a subcutaneous pocket and then pulled out. The hydrogel was placed on the spatula and inserted together into the subcutaneous pocket. The spatula was slowly retracted, while the hydrogel remained inside. The incised skin was sutured using a 6-0 nylon suture. For the fiber-connected hydrogel waveguide, a part of the scalp was incised and periosteum was retracted gently using Kimwipes. The optical fiber was fixed on the exposed skull by a drop of dental cement (GC Fuji I, GC America).

### Histology

A full-thickness skin around the hydrogel implant was excised and fixed in 4% formalin for 48 hours or longer. The skin sample is frozen-sectioned with 5- $\mu\text{m}$  thickness and stained with hematoxylin and eosin (H&E). The slide was imaged with a bright-field microscope (Olympus) with a 10 $\times$  objective lens.

### Optical setup

A fiber-coupled light emitting diode (LED;  $\lambda = 455 \text{ nm}$ ; M455F1, Thorlabs) was coupled to a hydrogel through fluorescence detection cube with dichroic cutoff at 500 nm (Doric lenses), and emission was measured using a spectrometer (Andor). For optogenetic stimulation, the output of the fiber-coupled LED was modulated to 0.1 Hz rectangular pulses with 50% duty cycle (5 s on followed by 5 s off) by using a function generator. Optogenetic cells in culture were illuminated at an intensity of 0.5  $\text{mW/cm}^2$  for 12 hours. To illuminate cells in the hydrogel waveguide implant, an average optical power of 1 mW was coupled into the pigtail fiber for 12 hours.

### Preparation of Q-dots

CdTe quantum dot was synthesized in house via hydrothermal route by reacting  $\text{Cd}^{2+}$  with NaHTe solution<sup>37</sup>. For  $\text{Cd}^{2+}$  solution, 2.35 mM of  $\text{Cd}(\text{ClO}_4)_2 \cdot 6\text{H}_2\text{O}$  (Sigma) was dissolved in 125 mL of distilled water, mixed with 5.7 mM of thioglycolic acid (Sigma), and adjusted to a pH of 11.6. For NaHTe solution, 1.2 mM of Te powder and 6 mM of  $\text{NaBH}_4$  (Sigma) were reacted in a three-necked flask by adding 5 ml of  $\text{N}_2$  saturated distilled water. The flask was heated to 60  $^\circ\text{C}$  under nitrogen gas purging until the color of the solution turned white. The prepared solutions were mixed to form CdTe precursor solution. The precursor solution was heated to 100  $^\circ\text{C}$  until its fluorescence emission reached 600 nm, and then the solvent was exchanged to PBS through isopropanol precipitation. CdSe/ZnS quantum dot with amphiphilic coating was purchased from Life Technologies (Qdot-605, Q21301MP).

### Cytotoxicity sensing

For the *in vitro* study, the cytotoxicity reporter cells were treated with CdSe/ZnS or CdTe at one day after transfection. The change in GFP expression was measured at 24 h after the treatment. For the animal study, cell-encapsulating hydrogels were implanted into 8-week-old Balb/c nude mice. One day after implantation, the baseline fluorescence was measured fiber-optically from the implant. Different groups of mice received intraperitoneal injections of PBS (100  $\mu$ l), CdSe/ZnS (100  $\mu$ l of 1  $\mu$ M in PBS), and CdTe quantum dots (100  $\mu$ l of 1  $\mu$ M in PBS), respectively. The fluorescence levels were measured at one and two days after the injection.

### Glucose tolerance test

To test the therapeutic efficacy of optogenetically secreted GLP-1, we used a chemically induced type-2 diabetes model prepared by the administration of low dose streptozotocin<sup>26</sup>. Briefly, 8-week-old Balb/c nude mice were pre-starved for 4 hours and received streptozotocin (40 mg/kg) diluted in 0.1 M citrate buffer (pH 4.5) for 5 consecutive days. For 6 days, 10% sucrose solution was provided in drinking water to prevent hypoglycemia. After 2 weeks, blood glucose level was measured using a digital glucose meter (Fora), and the blood glucose level higher than 250 mg/dl was considered as a diabetic condition. For the glucose tolerance test, mice were starved for 6 hours, and the baseline glucose levels were measured. After administering 1.5 g/kg of glucose intraperitoneally, the blood glucose levels were measured by titration at 15 min, 30 min, 60 min, 90 min and 120 min after the glucose injection. All animal experiments were performed in compliance with institutional guidelines and approved by the subcommittee on research animal care at the Massachusetts General Hospital.

### Data analysis

ImageJ was used for image processing and data quantification. Data were expressed as the means  $\pm$  SEM. Statistical analyses were performed using Graph Pad Prism software. Statistical differences were analyzed by t-test where indicated. P-value less than 0.05 was considered to be statistically significant.

### Supplementary Material

Refer to Web version on PubMed Central for supplementary material.

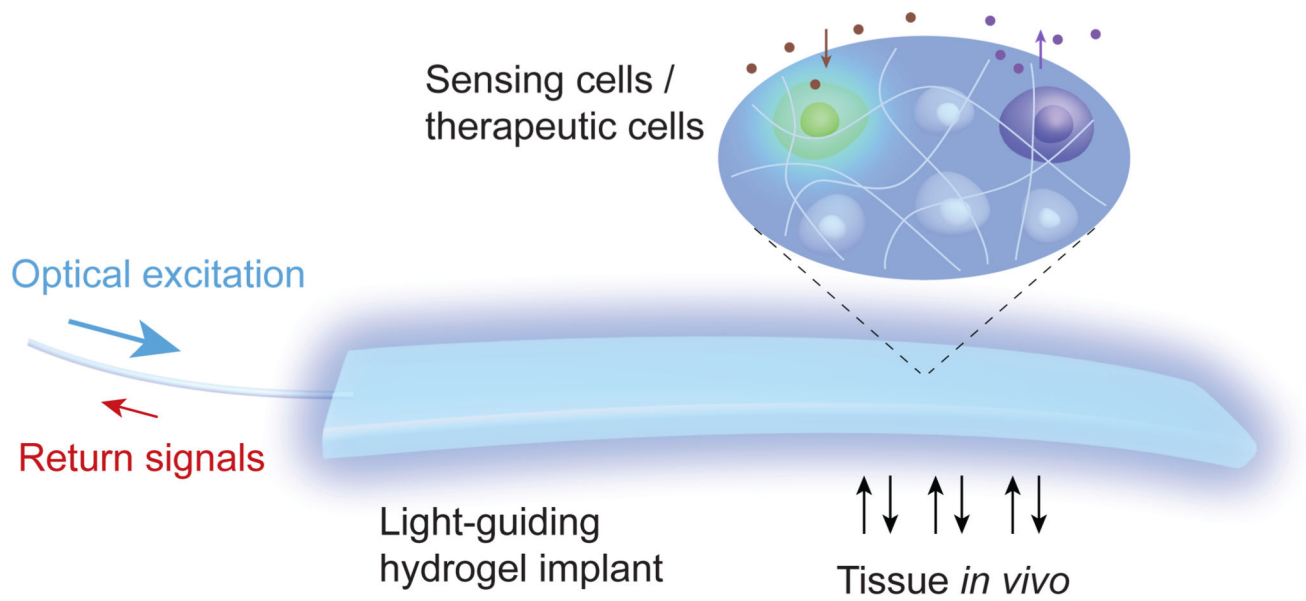
### Acknowledgement

We thank Martin Fussenegger and Haifeng Ye (ETH, Switzerland) for providing plasmids for optogenetic experiments. This work was funded by the U.S. National Institutes of Health (R21 EB013761), U.S. National Science of Foundation (ECS-1101947), U.S. Department of Defense (FA9550-10-1-0537), the IT Consilience Creative Program of MKE and NIPA (C1515-1121- 0003), and the Bio & Medical Technology Development Program and the World Class University Program of the Korean National Research Foundation (No. 2012M3A9C6049791, R31-2008- 000-10071-0). S.N. acknowledges financial support from the Bullock-Wellman Fellowship.

## References

1. Miller-Jensen K, Janes KA, Brugge JS, Lauffenburger DA. Common effector processing mediates cell-specific responses to stimuli. *Nature*. 2007; 448:604–608. [PubMed: 17637676]
2. Pancrazio JJ, Whelan JP, Borkholder DA, Ma W, Stenger DA. Development and application of cell-based biosensors. *Ann Biomed Eng*. 1999; 27:697–711. [PubMed: 10625143]
3. Banerjee P, Bhunia AK. Mammalian cell-based biosensors for pathogens and toxins. *Trends Biotechnol*. 2009; 27:179–188. [PubMed: 19187988]
4. El-Ali J, Sorger PK, Jensen KF. Cells on chips. *Nature*. 2006; 442:403–411. [PubMed: 16871208]
5. Zhang F, et al. Optogenetic interrogation of neural circuits: technology for probing mammalian brain structures. *Nat Protoc*. 2010; 5:439–456. [PubMed: 20203662]
6. Giepmans BN, Adams SR, Ellisman MH, Tsien RY. The fluorescent toolbox for assessing protein location and function. *Science*. 2006; 312:217–224. [PubMed: 16614209]
7. Rider TH, et al. AB cell-based sensor for rapid identification of pathogens. *Science Signalling*. 2003; 301:213.
8. Fenno L, Yizhar O, Deisseroth K. The development and application of optogenetics. *Annu Rev Neurosci*. 2011; 34:389–412. [PubMed: 21692661]
9. Ye H, Daoud-El Baba M, Peng RW, Fussenegger M. A synthetic optogenetic transcription device enhances blood-glucose homeostasis in mice. *Science*. 2011; 332:1565–1568. [PubMed: 21700876]
10. Wang X, Chen X, Yang Y. Spatiotemporal control of gene expression by a lightswitchable transgene system. *Nat Methods*. 2012; 9:266–269. [PubMed: 22327833]
11. Toettcher JE, Gong D, Lim WA, Weiner OD. Light-based feedback for controlling intracellular signaling dynamics. *Nat Methods*. 2011; 8:837–839. [PubMed: 21909100]
12. Kim M, et al. Maximal energy transport through disordered media with the implementation of transmission eigenchannels. *Nature Photonics*. 2012; 6:583–587.
13. Kwon K, Son T, Lee KJ, Jung B. Enhancement of light propagation depth in skin: cross-validation of mathematical modeling methods. *Lasers Med Sci*. 2009; 24:605–615. [PubMed: 19030946]
14. Sparta DR, et al. Construction of implantable optical fibers for long-term optogenetic manipulation of neural circuits. *Nat Protoc*. 2012; 7:12–23. [PubMed: 22157972]
15. Zhao S, et al. Cell type-specific channelrhodopsin-2 transgenic mice for optogenetic dissection of neural circuitry function. *Nat Methods*. 2011; 8:745–752. [PubMed: 21985008]
16. Hoffman AS. Hydrogels for biomedical applications. *Adv Drug Deliv Rev*. 2002; 54:3–12. [PubMed: 11755703]
17. Jain A, Yang AHJ, Erickson D. Gel-based optical waveguides with live cell encapsulation and integrated microfluidics. *Optics Letters*. 2012; 37:1472–1474. [PubMed: 22555708]
18. Wang Y, et al. Biosensor based on hydrogel optical waveguide spectroscopy. *Biosens. Bioelectron*. 2010; 25:1663–1668. [PubMed: 20044244]
19. Lee SC, Kwon IK, Park K. Hydrogels for delivery of bioactive agents: a historical perspective. *Adv Drug Deliv Rev*. 2013; 65:17–20. [PubMed: 22906864]
20. Kloxin AM, Tibbitt MW, Anseth KS. Synthesis of photodegradable hydrogels as dynamically tunable cell culture platforms. *Nat Protoc*. 2010; 5:1867–1887. [PubMed: 21127482]
21. Tibbitt MW, Anseth KS. Hydrogels as extracellular matrix mimics for 3D cell culture. *Biotechnol Bioeng*. 2009; 103:655–663. [PubMed: 19472329]
22. Lin S, Sangaj N, Razafiarison T, Zhang C, Varghese S. Influence of physical properties of biomaterials on cellular behavior. *Pharm Res*. 2011; 28:1422–1430. [PubMed: 21331474]
23. Choi W, et al. Tomographic phase microscopy. *Nat Methods*. 2007; 4:717–719. [PubMed: 17694065]
24. Taniguchi A. Live cell-based sensor cells. *Biomaterials*. 2010; 31:5911–5915. [PubMed: 20478614]
25. Drucker DJ. Glucagon-like peptides. *Diabetes*. 1998; 47:159–169. [PubMed: 9519708]
26. Wang Z, Gleichmann H. GLUT2 in pancreatic islets: crucial target molecule in diabetes induced with multiple low doses of streptozotocin in mice. *Diabetes*. 1998; 47:50–56. [PubMed: 9421374]

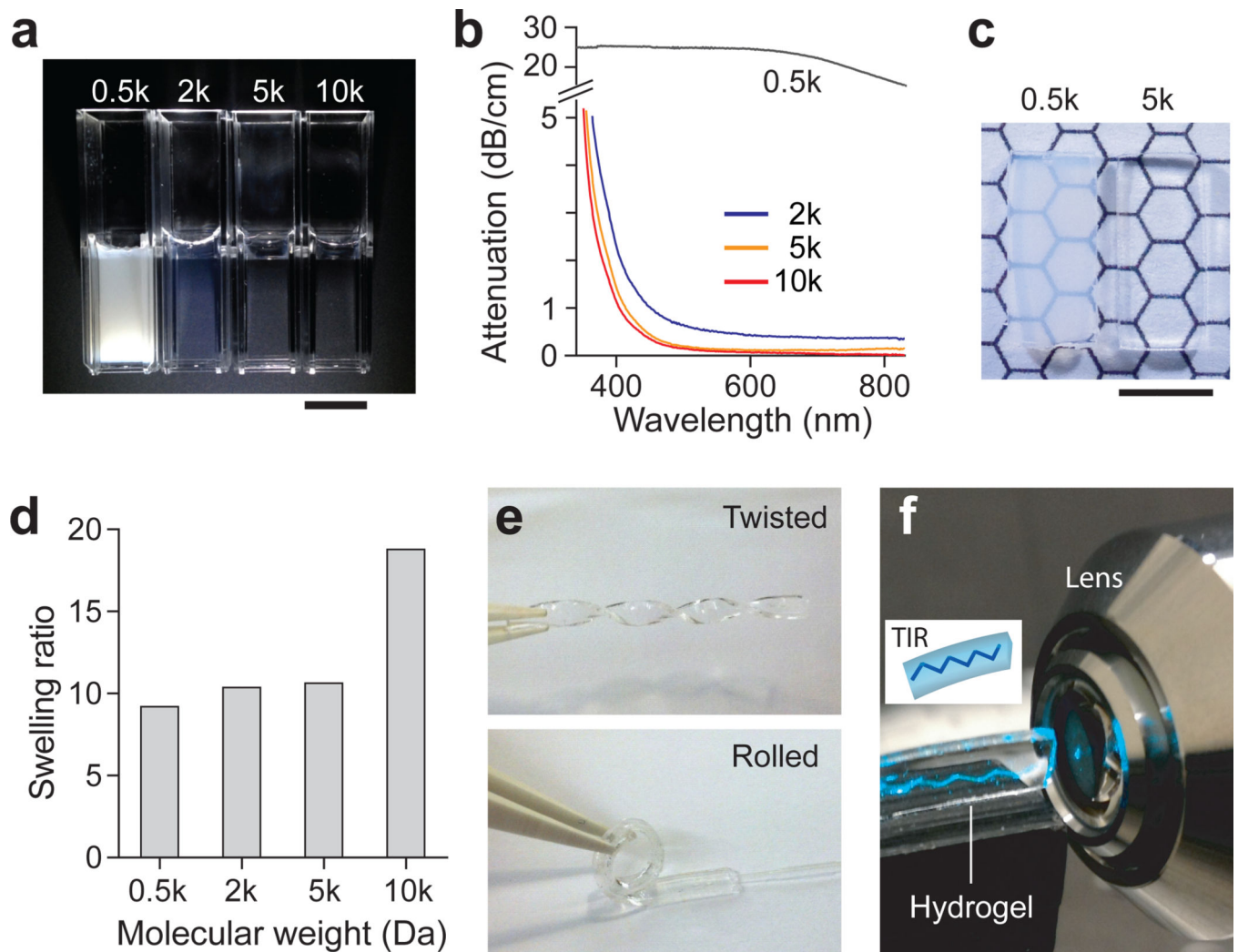
27. Parker ST, et al. Biocompatible silk printed optical waveguides. *Advanced Materials*. 2009; 21:2411–2415.
28. Dupuis A, et al. Prospective for biodegradable microstructured optical fibers. *Optics Letters*. 2007; 32:109–111. [PubMed: 17186033]
29. Wu Y-H, Park HB, Kai T, Freeman BD, Kalika DS. Water uptake, transport and structure characterization in poly (ethylene glycol) diacrylate hydrogels. *Journal of Membrane Science*. 2010; 347:197–208.
30. Yu L, Ding J. Injectable hydrogels as unique biomedical materials. *Chem Soc Rev*. 2008; 37:1473–1481. [PubMed: 18648673]
31. Slaughter BV, Khurshid SS, Fisher OZ, Khademhosseini A, Peppas NA. Hydrogels in regenerative medicine. *Adv Mater*. 2009; 21:3307–3329. [PubMed: 20882499]
32. Murua A, et al. Cell microencapsulation technology: towards clinical application. *J Control Release*. 2008; 132:76–83. [PubMed: 18789985]
33. Wurm FM. Production of recombinant protein therapeutics in cultivated mammalian cells. *Nat Biotechnol*. 2004; 22:1393–1398. [PubMed: 15529164]
34. Eyrich D, et al. Long-term stable fibrin gels for cartilage engineering. *Biomaterials*. 2007; 28:55–65. [PubMed: 16962167]
35. Sharma B, et al. Human cartilage repair with a photoreactive adhesive-hydrogel composite. *Sci Transl Med*. 2013; 5:167ra166.
36. Holtz JH, Asher SA. Polymerized colloidal crystal hydrogel films as intelligent chemical sensing materials. *Nature*. 1997; 389:829–832. [PubMed: 9349814]
37. Ge S, Zhang C, Zhu Y, Yu J, Zhang S. BSA activated CdTe quantum dot nanosensor for antimony ion detection. *Analyst*. 2010; 135:111–115. [PubMed: 20024189]



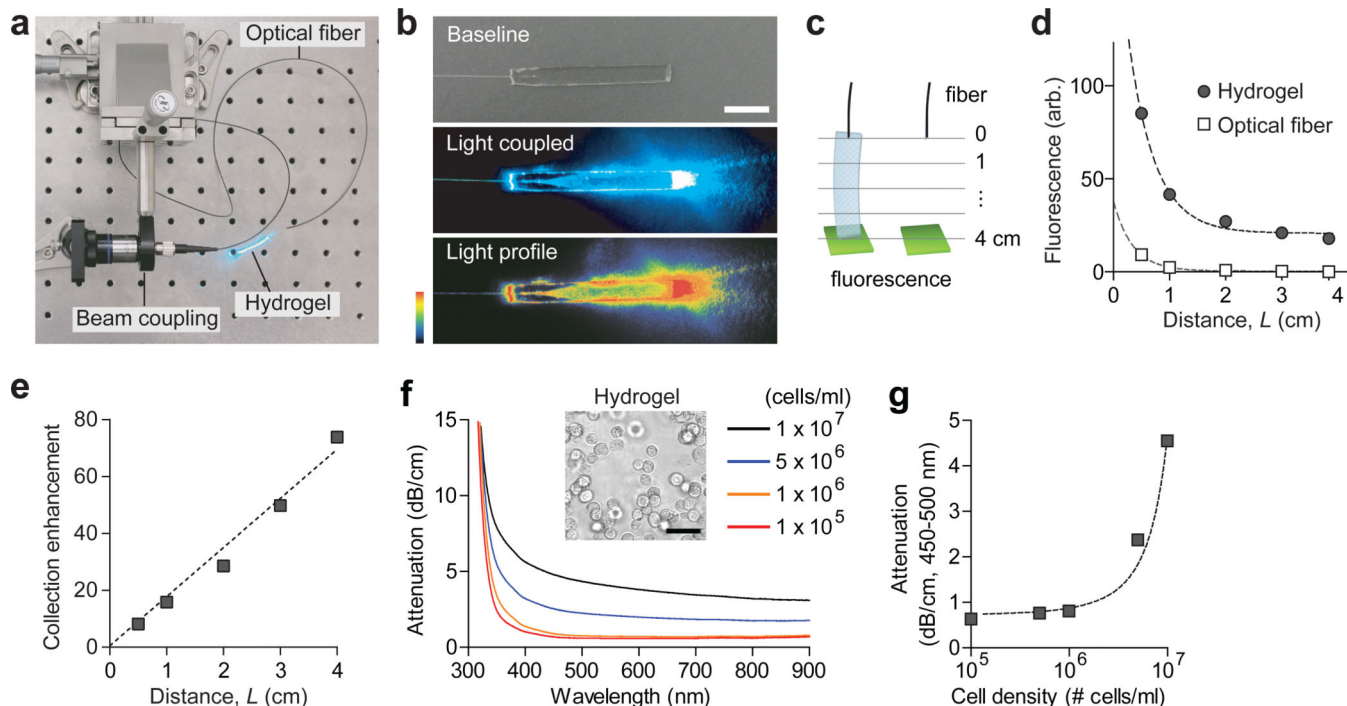
**Figure 1.**

Schematic of a light-guiding hydrogel encapsulating cells for *in vivo* sensing and therapy. The cells in the implanted hydrogel produce luminescence in response to environmental stimuli (sensing) and secrete cytokines and hormones upon photo-activation (therapy). The light guiding hydrogel establishes a bi-directional optical communications with the cells, allowing real-time interrogation and control of the biological system *in vivo*.



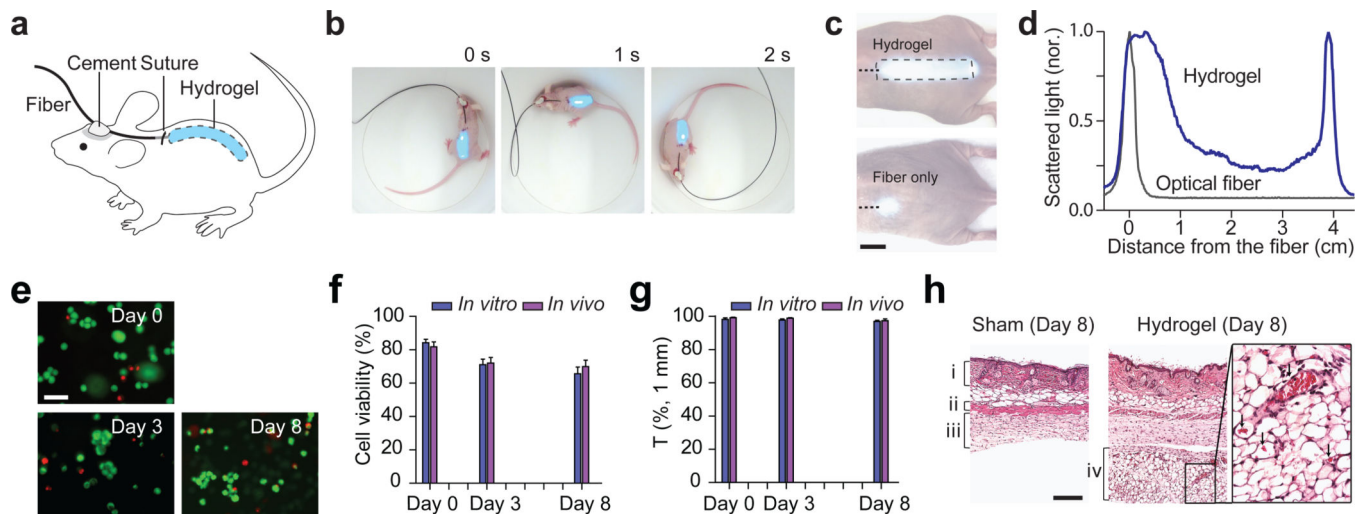


**Figure 2.** Characteristics of hydrogels. **(a)** Photographs of PEG-based hydrogels prepared by using 10% w/v PEGDA solution with different MW's of 0.5, 2, 5, and 10 kDa, respectively. Scale bar, 1 cm. **(b)** The optical attenuation spectra of PEG hydrogels prepared with different MW's of PEGDA. **(c)** Rectangular-shaped 0.5- and 5-kDa hydrogels with a thickness of 1 mm. Scale bar, 5 mm. **(d)** Swelling ratios of PEG hydrogels. The swelling ratio was calculated by dividing weight of swollen hydrogel by weight of dried hydrogel ( $n = 3$ ). **(e)** Mechanical flexibility of the PEG hydrogel (5 kDa, 10%). **(f)** Demonstration of total internal reflection within the slab hydrogel.



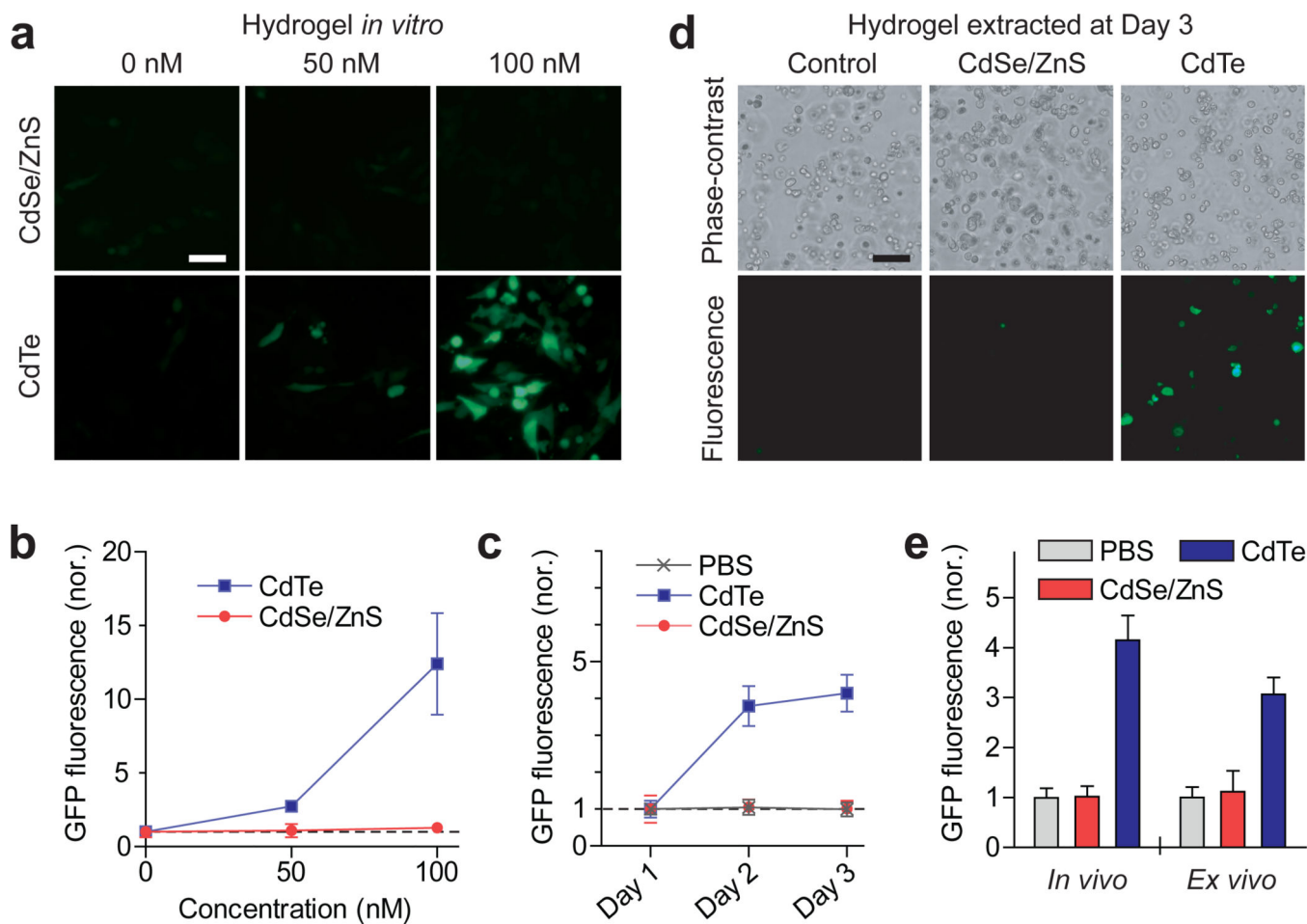
**Figure 3.**

Light-guiding properties of fiber-optic hydrogels. **(a)** A setup for coupling light into a hydrogel waveguide via a multimode fiber. **(b)** Photographs showing light coupling to a hydrogel. Top, a hydrogel before light coupling; middle, a hydrogel after light coupling; and bottom, a pseudo color image for spatial profile of scattered light. **(c)** Schematic of the setup for measuring the collection efficiency. A fluorescent sample (green) was placed in contact with hydrogels with varying lengths (left) or at the equivalent distances from a multimode fiber (right). **(d)** Magnitude of fluorescence collected into the optical fibers with and without the hydrogels. Dashed lines, curve fit with  $1/L^2$  and  $1/L$  dependence for the hydrogel and optical fiber alone, respectively. **(e)** The ratio of fluorescence with and without the hydrogels. The dashed line represents a linear regression ( $R^2 = 0.98$ ). **(f)** The optical attenuation spectra of the hydrogels at various cellular density levels. Inset shows a phase-contrast micrograph of the hydrogel. Scale bar, 50  $\mu\text{m}$ . **(g)** Average optical attenuation of a hydrogel with  $1 \times 10^6$  cells/cm<sup>3</sup> in a spectral range of 450–500 nm. The dashed line shows an exponential fit ( $R^2 = 0.96$ ).



**Figure 4.**

Hydrogel implants *in vivo*. **(a)** Schematic of a fiber-pigtailed hydrogel waveguide implanted in a mouse. **(b)** A hydrogel-implanted mouse in a freely moving state. Blue light (491 nm) was coupled. **(c)** Photographs showing the light scattering profiles from an optical hydrogel implant (left) and from an optical fiber (right). **(d)** Axial profiles of the magnitude of scattered light from the hydrogel implant (blue) and the optical fiber only (black). **(e)** Fluorescence images of hydrogel implants immediately after taken out of mice at 3 days and 8 days after implantation, in comparison to control (Day 0; prior to implantation). Live cells emit green fluorescence from a membrane-permeable live-cell staining dye, calcein-AM, and dead cells are identified by red fluorescence from ethidium bromide in the cell nuclei. Scale bar, 50 μm. **(f)** Long-term viability of the encapsulated cells *in vivo*. Error bars are standard deviations (n = 6 each). **(g)** Change in optical transmittance of the hydrogel implants *in vivo*. **(h)** H&E histology images of the skin tissues examined at 8 days after implantation, showing (i) dermis, (ii) panniculus carnosus, (iii) subcutaneous loose connective tissue layer, (iv) newly formed connective tissue layer. In the magnified image (right), arrows indicate red blood cells in blood vessels. Scale bar, 100 μm.

**Figure 5.**

Cell-based sensing of nano-cytotoxicity of quantum dots. **(a,b)** Fluorescence images of the sensor cells in hydrogels *in vitro* at two days after adding CdTe and CdSe/ZnS Q-dots, respectively, into the medium. Scale bar, 20  $\mu\text{m}$ . **(b)** The magnitude of green fluorescence from the hydrogels, measured through the pigtail fibers. **(c)** *In vivo* measurement of the fluorescence signals from the sensing cells in hydrogels implanted in live mice. Q-dots were administered by intravenous injection 24 hours after the hydrogels were implanted. **(d)** Fluorescence images of the hydrogels extracted from the mouse at day 3. Scale bar, 20  $\mu\text{m}$ . **(e)** Comparison of the GFP fluorescence measured fiber-optically *in vivo* (left) and fluorescence microscopy *ex vivo* (right).

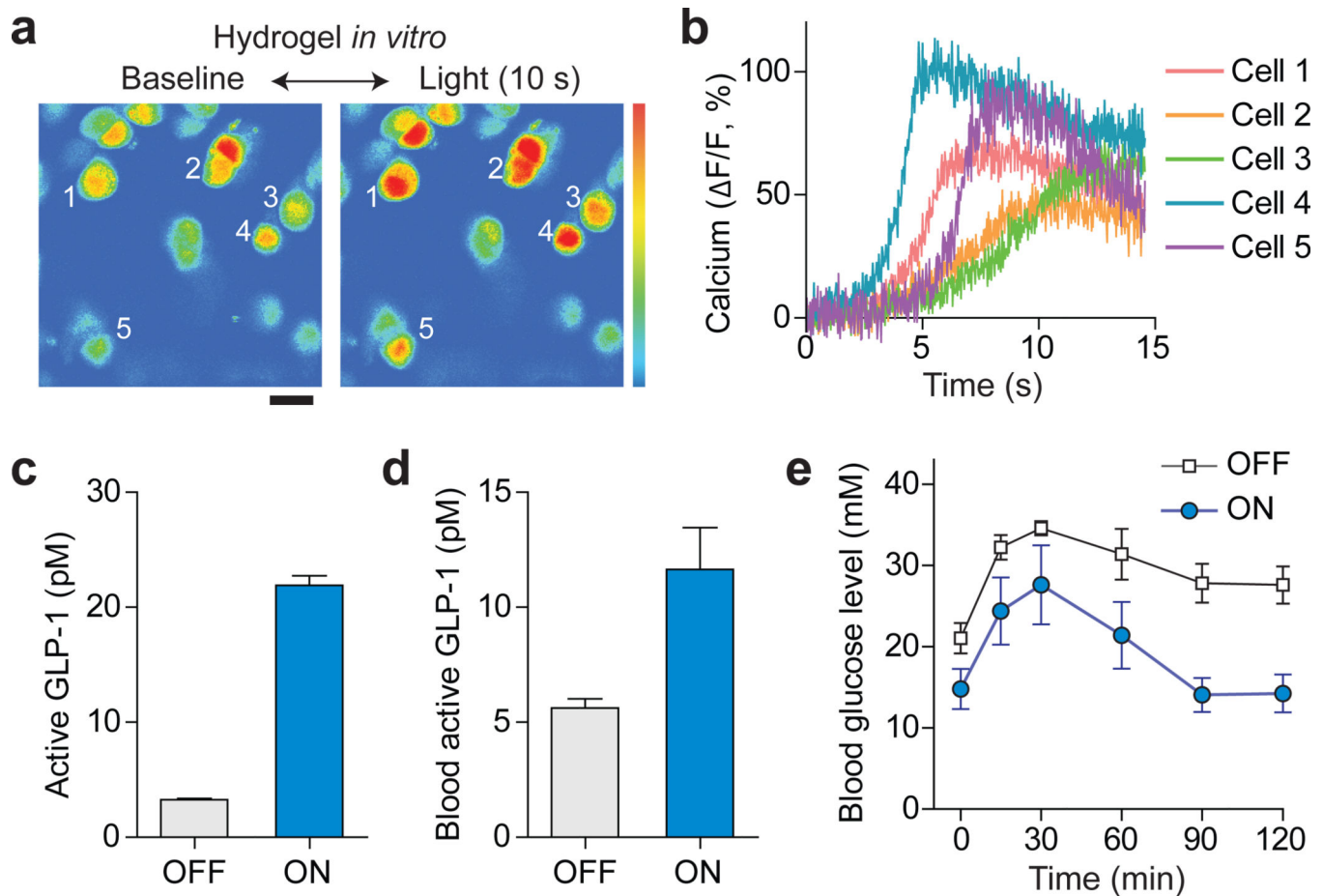


**Figure 6.**

Optogenetic therapy in a mouse model of diabetes. **(a)** Fluorescence calcium-level imaging of optogenetic cells in a hydrogel waveguide *in vitro*. Upon delivering blue light (455 nm) through the fiber for 10 s at 1 mW, the fluorescence from an intracellular calcium indicator, OGB1-AM increased significantly. Scale bar, 20  $\mu\text{m}$ . **(b)** Time traces of intracellular calcium signals from various cells marked in **(a)**. **(c)** Concentrations of active GLP-1 in the medium of hydrogels with (ON) and without (OFF) providing the activation light. **(d)** Level of GLP-1 in blood plasma measured *in vivo* at 2 days after light exposure. **(e)** Blood glucose levels in the chemically induced diabetic mice with and without delivering activation light. Error bars, standard deviations ( $n = 4$ ).